PAPER

CrossMark
click for updates

Spatial quenching of a molecular charge-transfer process in a quantum fluid: the Cs_x–C_{60} reaction in superfluid helium nanodroplets†

Andreas W. Hauser*[a] and María Pilar de Lara-Castells*[b]

A recent experimental study [Renzler *et al.*, *J. Chem. Phys.*, 2016, **145**, 181101] on superfluid helium nanodroplets reported different reactivities for Cs atoms and Cs_2 dimers with C_{60} fullerenes inside helium droplets. Alkali metal atoms and clusters are heliophobic, therefore typically residing on the droplet surface, while fullerenes are fully immersed into the droplet. In this theoretical study, which combines standard methods of computational chemistry with orbital-free helium density functional theory, we show that the experimental findings can be interpreted in the light of a quenched electron-transfer reaction between the fullerene and the alkali dopant, which is additionally hindered by a reaction barrier stemming from the necessary extrusion of helium upon approach of the two reactants.

1 Introduction

He-nanodroplets, a common tool for spectroscopy of atoms and molecules in a weakly perturbing matrix,[1–4] have been suggested as nanolabs for the study of reactions at lowest temperatures. Most molecules submerge into these droplets after collision due to the stronger interactions between the dopant and He than between the He atoms themselves. However, alkali metal atoms and their smallest clusters tend to stay on the droplet surface since their diffuse electronic distribution would displace too much helium, making a complete submersion energetically unfeasible.[5,6]

Recently, the interaction between a heliophilic C_{60} molecule, known to reside inside a He droplet, with a heliophobic Cs atom or a Cs_2 dimer has been studied experimentally.[7] These experiments indicate that the subsequential doping of a C_{60}-doped He-droplet with a single Cs atom does not to lead to a reaction between the two dopants, while a reaction between the heliophilic and the heliophobic dopants takes place in cases where Cs_2 is formed on the droplet beforehand. In other words, only if the doping rate with alkali atoms in the experiment is high enough for dimerization a direct reaction on the droplet can be observed.

In this theoretical study, we describe this phenomenon observed by our colleagues *via* a combination of electronic structure calculations and orbital-free, bosonic helium density functional theory. One-dimensional potential energy scans are generated as approximations to the reaction pathway describing the interaction between a single Cs atom or an alkali metal dimer and a C_{60} fullerene. These curves, calculated for the free-gas situation, are then corrected for the interaction with the surrounding helium. A similar study on the interaction of a heliophilic and a heliophobic dopant has been performed for the Xe–Rb system.[8] However, in the current case, the very high polarizability of the fullerene, together with its high electron affinity, gives rise to two new features: first, the dissociation energies for Cs–C_{60} and Cs–C_{60} lie in the range of about 2 eV due to the ionic character of the interaction. Therefore, strong attractive interaction is to be expected between a submerged, heliophilic fullerene and the surface-residing, heliophobic Cs atoms. Second, the high polarizability of C_{60} leads to a strong van der Waals interaction between the fullerene and its surrounding helium. As a consequence, the helium density, spherically distributed around the C_{60} molecule in the droplet center, will have a highly peaked radial maximum near the cavity surface. The aim of this article is to show that the extrusion of helium from these areas of high density, together with a reduced mobility due to the He environment, causes an energy penalty high enough to form reaction barriers which can explain the recent experimental findings.

2 Computational methods

2.1 *Ab initio* calculations

The interaction of a C_{60} molecule with a single Cs atom and a Cs dimer in its singlet and triplet spin states is studied using (electronic) density functional theory. For carbon we used the

[a] *Graz University of Technology, Institute of Experimental Physics, Petersgasse 16, 8010 Graz, Austria. E-mail: andreas.w.hauser@gmail.com*

[b] *Instituto de Física Fundamental, CSIC, Serrano 123, 28006 Madrid, Spain. E-mail: Pilar.deLara.Castells@csic.es*

† Electronic supplementary information (ESI) available: A series of additional He density graphs, details of the MCSCF approach, fully repulsive CDFT curves, a table with the parameters of the pairwise potential model and figures documenting the quality of the fitting approach. See DOI: 10.1039/c6cp06858h

Def2-SVP basis set.[9] For cesium, the Def2-QZVP basis set of the same family[10] was combined with the ECP46MDF effective core potential of the Stuttgart/Köln group.[11] We further chose the cost-efficient B97M-V functional, a recent development of the Head-Gordon group,[12] which combines a combinatorially-optimized semi-local meta-GGA exchange–correlation functional[13] with the VV10 nonlocal correlation functional.[14] This density functional approach has been thoroughly tested on several standard databases and shows remarkable accuracy for the prediction of non-bonded interactions and atomization energies at minimal computational cost, which makes it a straight-forward choice for the given task. Although higher levels of theory and larger basis sets would be applicable to the moderately sized, isolated Cs dimer in principle, DFT calculations using the same functional and the same quadruple-zeta basis set were performed for the sake of internal consistency. All Cs_x–C_{60} curves have been corrected for basis superposition errors due to the significant difference in the basis set size on each fragment.[15] The correction gives rise to geometry shifts in the range of about 0.05 Å. For improved SCF convergence, the pseudo-fractional occupation number method of Rabuck and Scuseria has been applied in all cases.[16]

In order to study the impact of the helium environment on charge mobility we further employ the constrained-DFT method of Wu and Van Voorhis[17] to analyze covalent and ionic contributions as well as two-state, wave function-based, multi-configurational SCF calculations (MCSCF),[18,19] aided by long-range dispersion corrections. The two-state MCSCF calculations provided both the electronic ground state, asymptotically correlated to $C_{60}^- + Cs_x^+$ fragments, and an excited electronic state which, in the long-range potential region, asymptotically correlated to neutral $C_{60} + Cs_x$ species. The necessary dispersion–correction corrections for the neutral state are extracted from the application of the CCSD(T) approach[20] to small model (Cs_x/benzene) systems. The MCSCF and CCSD(T) calculations comprise a slightly altered basis set for the carbon atoms and a fitting of long-range correlation energies for improved accuracy. The details are given in both the Appendix and the ESI.†

All calculations are performed using the Q-Chem program package[21] with the exception of the MCSCF and preliminary CCSD(T) calculations, for which the Molpro suite of programs[22] is used.

2.2 He density functional theory

Free energies of doped He nanodroplets (He_N) are obtained via helium density functional theory (He-DFT) based on a slightly modified version of the Orsay–Trento density functional.[29,30] Note that in contrast to common DFT approaches such as the one discussed above, this functional maps the helium density onto the energy and not the electron density. The free energy of a doped He droplet is minimized with respect to a given arrangement of the dopants within the droplet and on its surface. The free energy $F[\rho]$, a functional of the helium density ρ, can be written as

$$F[\rho] = E[\rho] + U_{ext}[\rho] - \mu N[\rho] - \mathbf{F} \cdot \mathbf{R}[\rho], \tag{1}$$

where $E[\rho]$ denotes the Orsay–Trento density functional and $U_{ext}[\rho]$ an external potential introducing the interaction between the droplet and the dopants. The necessary ingredients for the generation of $U_{ext}[\rho]$ will be discussed in Section 3.5. Note that interactions between the dopants themselves are not part of the simulation and need to be added a posteriori. The remaining terms of eqn (1) are a consequence of the two constraints imposed on the minimization procedure: the conservation of N, the particle number, and $\mathbf{R}$, the He droplet mass center. Both can be written as functionals of the density,

$$N = \int d\mathbf{r}\rho(\mathbf{r}), \quad \mathbf{R} = \frac{1}{N}\int d\mathbf{r}\rho(\mathbf{r})\mathbf{r}. \tag{2}$$

Their corresponding Lagrange parameters are the chemical potential μ and the retaining force $\mathbf{F}$, respectively. The density functional itself can be written as[30]

$$\begin{aligned} E[\rho] &= \frac{\hbar^2}{2m}\int d\mathbf{r}\left(\nabla\sqrt{\rho(\mathbf{r})}\right)^2 \\ &+ \frac{1}{2}\int d\mathbf{r}d\mathbf{r}' V_{LJ}(|\mathbf{r} - \mathbf{r}'|)\rho(r)\rho(r') \\ &+ \frac{c_2}{2}\int d\mathbf{r}\rho(\mathbf{r})\bar{\rho}(\mathbf{r})^2 + \frac{c_3}{2}\int d\mathbf{r}\rho(\mathbf{r})\bar{\rho}(\mathbf{r})^3 \\ &+ C\int d\mathbf{r}[1 + \tanh(\beta\{\rho(\mathbf{r}) - \rho_m\})], \end{aligned} \tag{3}$$

with the first term as the quantum kinetic energy, the second as a Lennard-Jones-type He–He pair potential interaction energy, terms 3 and 4 as short range correlation energy contributions involving $\bar{\rho}$, a locally averaged density for a given sphere of radius $\bar{h}$, and finally, a penalty term which forbids an extra pile-up of He density as soon as the density exceeds a threshold value ρ_m. Note that an additional, nonlocal kinetic energy term which appears in the original formulation (proportional to $\nabla\rho(\mathbf{r})\rho(r')$) has been dropped here for stability reasons. For details, we refer to ref. 30 and 31, where this type of functional has been used to study the freezing transition of superfluid helium at high pressure.

3 Results and discussion

3.1 C_{60} interacting with Cs_2

In a first step, the geometry of the Cs dimer was optimized in the singlet and triplet spin states using the chosen density functional. The resulting binding energies and equilibrium bond lengths show a reasonable agreement with the experimental data and previous ab initio studies performed at a higher level of theory (see Table 1). Note, however, that our results are obtained at a fraction of the typical computational cost, which allows us to extend our study towards the interaction with a C_{60} fullerene. We approach the dimer with a single C_{60} molecule[32] on a straight trajectory perpendicular to the internuclear axis of the dimer and along the C_3 axis of the fullerene. This choice of relative positioning (referred to as T-shaped) reflects the typical adsorption geometry for high-spin alkali dimers on the surface of helium droplets.[33,34] We calculate the energy of the system as a function of the distance between both centers of mass. The one-dimensional energy

This journal is © the Owner Societies 2017

Phys. Chem. Chem. Phys., 2017, **19**, 1342–1351 | **1343**

Table 1 Characteristics of the Cs_2 dimer potential curves and comparison to previous studies

State	r_{min} (Å)	E (cm^{-1})	Ref.	Method
$X^1\Sigma_g^+$	4.73	4908		This study
	4.64	3648	23 and 24	Experiment
	4.695	3194	25	DFT
	4.75	4275	26	DFT
$a^3\Sigma_u^+$	6.47	246		This study
	6.30	295	27	Exp./full CI, 2 el.
	6.640	237	28	Coupled cluster

surfaces plotted in Fig. 1 can be interpreted as a first approximation to the reaction pathways for the interaction of Cs_2 with a single C_{60} molecule. They are calculated for both spin manifolds, with the Cs–Cs distance kept at the corresponding minimum energy value. The binding energies and equilibrium distances are listed in Table 2.

Our findings are in qualitative agreement with previous studies on the related Na_2–C_{60} system,[35] which also shows a deeper minimum for the triplet state. As a consequence, both spin states must cross at a certain distance, since for a free Cs_2 molecule the singlet state PES has a deeper minimum than the triplet state (see Table 1). From our current results, the crossing takes place in the potential minimum region of the singlet state (*ca.* 6 Å). This can be seen if the triplet state of Cs_2 in Fig. 1 is mentally shifted to higher energies by the singlet–triplet energy difference of the free gas dimer (4662 cm^{-1}). The Cs–C_{60} system seems to approach its asymptotic value slightly faster, which indicates a less pronounced interaction in the long range. The different behaviors of the dispersion-dominated tails are easily understood by considering that the value of the average polarizability for triplet Cs_2 (*ca.* 868 a.u. from ref. 36) is twice as large as that of atomic Cs (*ca.* 401 a.u. from ref. 37).

For the sake of completeness, we repeated our scans also for a collinear arrangement of the Cs_2 molecule in both spin states, with the internuclear axis parallel to the C_3 axis of the fullerene. The corresponding one-dimensional energy surfaces are plotted in Fig. 2. For this geometry, the binding energies are reduced significantly, in particular for the triplet dimer. Again, the distance is measured from the fullerene center to the center of mass of the Cs_2 dimer. Note that the different dimer bond lengths of the $X^1\Sigma_g^+$ ground state and the $a^3\Sigma_u^+$ state lead to minima at significantly different intermolecular distances in this geometry arrangement.

3.2 C_{60} interacting with a single Cs atom

We further compare both spin manifolds of the dimer (and both relative arrangements, *i.e.* T-shaped and collinear) to the interaction of C_{60} with a single alkali atom in its doublet ground state. The corresponding potential depth and minimum position differ considerably from that of the triplet dimer resulting in a T-shaped arrangement, showing about half the binding energy at a much larger distance (see Fig. 1 and 2). The singlet dimer in the T-shaped configuration is also stronger bound than a single atom, while the singlet dimer in a collinear configuration shows an even smaller binding energy than that of the single Cs atom.

For the T-shaped configuration, the curvature of the Cs–C_{60} PES becomes similar to the curvatures of Cs_2–C_{60} in the mid- to long-range. However, the comparably shallow potential minimum and the lack of sufficiently attractive forces at larger distances are already pointing towards an explanation for the quenched reactivity of a single Cs atom when compared to the triplet Cs_2 dimer.

3.3 Ionization energies and Mulliken charges

The high electron affinity of the fullerene makes the interaction with the Cs atom clearly ionic in character. For Cs–C_{60}, we obtain

Table 2 Characteristics of the C_{60} interaction curves, with the dimer internuclear axis perpendicular (T-shaped) or parallel (collinear) to the C_3 axis of the fullerene. All asymptotes are set to zero for an infinite distance between the fullerene and Cs_x

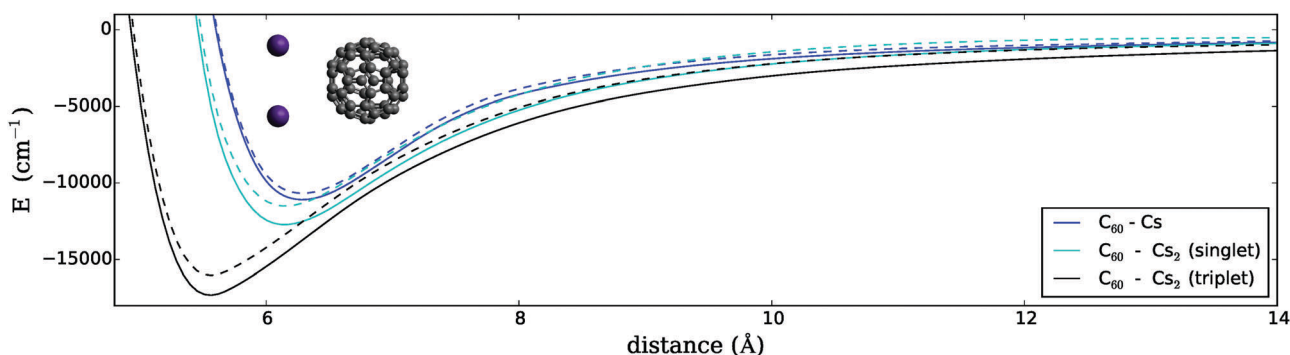| Interaction	State	r_{min} (Å)	E (cm^{-1})
Cs–C_{60}	$^2S_{1/2}$	6.27	11 087
Cs_2–C_{60}	$X^1\Sigma_g^+$ (T-shaped)	6.12	12 716
Cs_2–C_{60}	$a^3\Sigma_u^+$ (T-shaped)	5.57	17 320
Cs_2–C_{60}	$X^1\Sigma_g^+$ (collinear)	8.73	8822
Cs_2–C_{60}	$a^3\Sigma_u^+$ (collinear)	9.53	11 176

Fig. 1 Potential curves for the Cs–C_{60} (doublet) and the Cs_2–C_{60} systems (singlet and triplet, in a T-shape configuration, *i.e.* with the Cs_2 internuclear axis perpendicular to the C_3 axis of the fullerene). Energies are plotted as a function of the distance between both centers of mass. The dashed lines correspond to blue potential energy surfaces (PESs) which are corrected for the spatial hindrance in superfluid helium; see Section 3.6 for details.
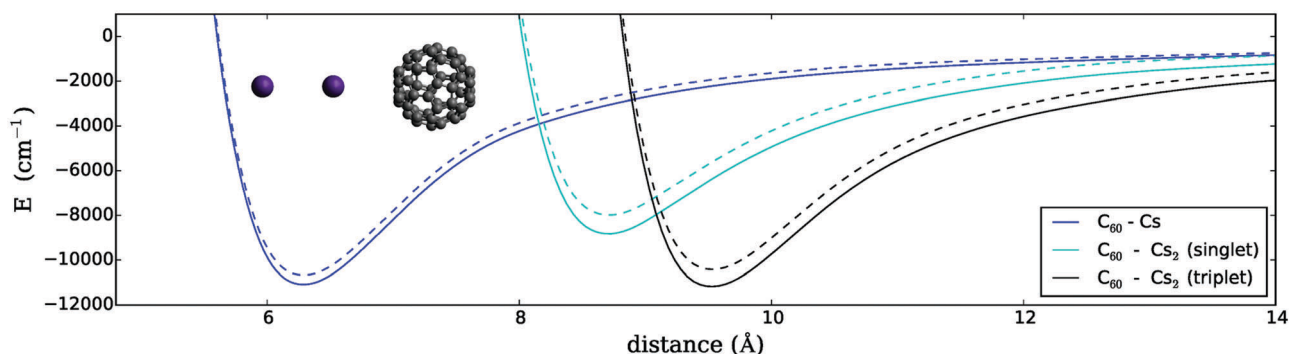
Fig. 2 Potential curves for the Cs–C_{60} (doublet) and the Cs_2–C_{60} systems (singlet and triplet, with the Cs_2 internuclear axis parallel to the C_3 axis of the fullerene). Energies are plotted as a function of the distance between both centers of mass. The dashed lines correspond to PESs which are corrected for the spatial hindrance in superfluid helium; see Section 3.6 for details.

Table 3 A comparison of Mulliken charges and ionization energies for Cs–C_{60} and Cs_2–C_{60} systems

Interaction	State	Charge on Cs/Cs_2 (e)	IE^a (eV)
Cs–C_{60}	$^2S_{1/2}$	0.80	3.56
Cs_2–C_{60}	$X^1\Sigma_g^+$ (T-shaped)	1.04	3.21
Cs_2–C_{60}	$a^3\Sigma_u^+$ (T-shaped)	1.50	2.83
Cs_2–C_{60}	$X^1\Sigma_g^+$ (collinear)	2.03, −1.20	3.32^b
Cs_2–C_{60}	$a^3\Sigma_u^+$ (collinear)	0.83, 0.07	3.18^b

^{a} Estimation based on the energy of the highest occupied orbitals. ^{b} The first value refers to the Cs atom which is closer to the fullerene.

a dipole moment of 17.5 D, which is in reasonably good agreement with the experimental value of 21.5 ± 2 D reported in ref. 38. An overview of Mulliken charges and ionization energies (IEs) estimated from the DFT calculations is given in Table 3. For a single Cs atom we observe a positive charge of $+0.80e$ at the Cs–C_{60} equilibrium position. In the case of the Cs_2 molecule in the T-shaped configuration, a transfer of $-1.5e$ onto the fullerene could be observed in the triplet state, while a reduced transfer of only $-1.04e$ occurs in the case of the singlet dimer. The ionization energies of 3.21 and 2.83 eV are significantly higher than those of the corresponding free Cs_2 molecules, for which we obtain 2.37 eV for the singlet and 1.96 eV for the triplet state, using the same computational approach. For the collinear geometry arrangement we also find higher ionization energies than for the free molecules (see Table 3). The Mulliken charges in this configuration are particularly interesting: while the total charge transfer in both spin states (about $-0.87e$ on average) is only slightly lower than for the T-shaped geometry, we find an extremely polarized Cs_2 molecule for the singlet state.

3.4 Cs_x–C_{60} curves without charge transfer

The previous sections revealed that the interaction of a single Cs atom or a Cs_2 molecule with a fullerene shows a strong ionic character. However, since both reactants are spatially separated by superfluid helium, a quenched electron mobility is to be expected. In this section, we approximate this feature by constraining both reactants to stay fully neutral upon approaching each other. To do this, we employ constrained-DFT,[17] (CDFT)

which allows introducing arbitrary constraints to the electron density during the self-consisted-field iterations of the DFT calculations. To each of these constraints corresponds a Lagrange multiplier V_c with the physical meaning of a fictitious external potential, which acts on the density in such a way that the neutrality of both reactants (Cs_x and the C_{60}) is assured. As a consequence, the additional potential expression occurs in the Kohn–Sham equations, and the corresponding orbitals are evaluated, together with V_c, in a self-consistent manner.

In our case, we enforce charge neutrality on both reactants, but also enforce a total spin of 1/2 to the Cs atom (or a total spin 1 to Cs_2 in the triplet state) in order to improve the convergence. Unfortunately, the so-obtained PES does not show bound states, neither for Cs nor for Cs_2. Since this will be of relevance for the future discussion of long-range dispersion interactions captured *via* DFT, we included the fully repulsive curves in the ESI.† For comparison, we repeated the CDFT calculations using the B97-D functional,[39] which contains an empirical *ad hoc* correction for van der Waals interactions, and the ωB97X-V, a hybrid functional[40] which is closely related to our original choice of B97M-V. None of them shows a bound state. The assumption of an attractive interaction which is difficult to retrieve is supported by a series of benchmark CDFT calculations on the C_6H_6–Cs model system, which is also not bound at the B97M-V level of theory if charge-neutrality on cesium and the benzene ring is enforced, but which shows a bound state in the CCSD(T) calculations, *i.e.* coupled cluster singles and doubles excitations with perturbative triples.[41]

Since the current system is too large for a constrained CCSD(T) calculation we fall back on the multi-configurational SCF (MCSCF) approach[18,19] but aided by the necessary long-range dispersion-type corrections in the neutral state. A minimal active space is chosen for the sake of computational feasibility. The long-range energy corrections have been extracted from CCSD(T) studies of the C_6H_6–Cs and C_6H_6–Cs_2 systems; details are given in the Appendix. Using this technique we obtained a more accurate PES for the two most intriguing systems of our study, *i.e.* a fullerene interacting with a triplet Cs_2 molecule in a T-shaped arrangement (by far the strongest interaction) or a single Cs atom (the weakest interaction). The results of these PES
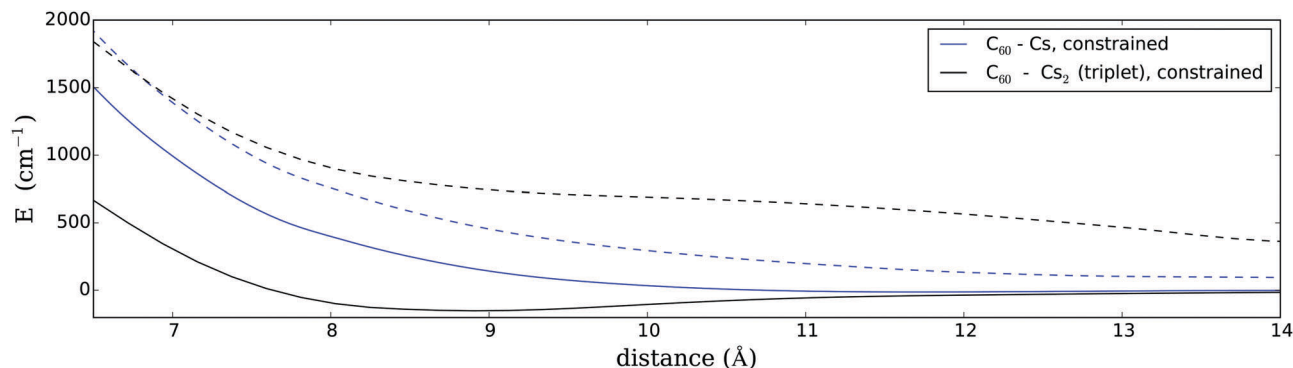
This journal is © the Owner Societies 2017

Phys. Chem. Chem. Phys., 2017, **19**, 1342–1351 | **1345**

Fig. 3 Fully covalent curves for Cs and Cs_2 interacting with C_{60}, maintaining charge neutrality on both reactants upon formation. The dashed lines correspond to PESs which are corrected for the spatial hindrance in superfluid helium; see Section 3.6 for details.

scans are plotted in Fig. 3. As can be seen, the exclusion of any charge transfer has an extreme quenching effect on attractive interactions. In fact, for a single Cs atom, the PES is still fully repulsive. For triplet Cs_2, on the other hand, we find a very shallow minimum of about 160 cm^{-1} at an equilibrium distance of 9 Å. Although this is only a small fraction of the original binding energy, it plays a big role in the overall reaction since it is comparable to the barrier created by spatial hindrance due to the helium environment. We will discuss the consequence of these findings in a later section.

3.5 Interactions between dopants and He

To obtain the last ingredients for the follow-up He-DFT calculation, the C_{60} fullerene is approached with a single He atom on a straight trajectory parallel to the C_3 axis. Here, we fall back on the results reported by Hesselmann and Korona,[42] who calculated the potential energy as a function of the He–C_{60} distance *via* symmetry-adapted perturbation theory with monomers described by density functional theory (DFT-SAPT).[43,44]

To obtain an accurate description of the medium to long-range part, which is crucial for our approach of pair-potential summation in the He-DFT code, we have fitted the DFT-SAPT energies to our new pairwise additive potential model for atom/C_{60} interactions. The basic outline of this approach can be found in the Appendix. A similar ansatz has been used by us recently to study the submersion of carbon nanotubes in superfluid helium.[45]

The resulting spherically averaged curve, which will be used for the generation of the total interaction potential of C_{60} and a helium droplet, is plotted in Fig. 4. It shows a minimum of 57 cm^{-1} at an equilibrium distance of 6.76 Å. From this comparably strong interaction with a single He atom (a value of 5 cm^{-1} is typically assumed for the binding energy per He atom in droplets[29]) we can derive already that a fullerene will not just fully immerse into the He droplet, but will be surrounded by a helium shell of high density, giving rise to a local phase transition from the liquid to a nonspherical, crystalline bulk structure. This well-known phenomenon has been termed 'snowball formation' in the He droplet community. However, the He–C_{60} interaction potential can be assumed to be spherically symmetric due to the high symmetry of the C_{60} fullerene,
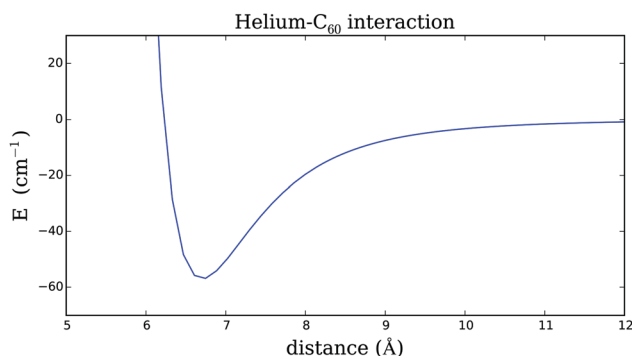

Fig. 4 One-dimensional plot of the pair potential for the interaction of He and a C_{60} fullerene. A spherically averaged model potential (see Appendix), fit to data points of ref. 42.

and a single curve documenting the radial dependence can be used for the generation of a He_N–C_{60} interaction potential *via* summation over pair potentials.

In order to obtain a reliable description of the weak interaction between Cs and the He environment, we use the analytical He–Cs potential provided in ref. 46. The corresponding curve is plotted in Fig. 5 for comparison. It shows a minimum of less than 1 cm^{-1} at a distance of 7.73 Å.

For the slightly more complex interaction between Cs_2 and the He droplet we fall back on the study of Prosmiti *et al.*,[47] which contains a very detailed analysis of the intermolecular potential energy surface for the He–Cs_2 system in the triplet state based on high level *ab initio* calculations. The authors have provided an analytical description of the surface as a function of r, the distance between the centers of mass of the two fragments (He and Cs_2), and the angle ϕ, measured between the internuclear axis of the Cs_2 molecule and the distance vector between the two centers of mass.

The two angles $\phi = 0°$ and $\phi = 90°$ have been selected for plots of the He–Cs_2 interaction energies as a function of the distance in Fig. 5. Note that the equilibrium distance for $\phi = 90°$, which corresponds to the T-shaped, perpendicular structure, represents the global minimum of the PES. For this geometry, a binding energy of about 2 cm^{-1} is reported in
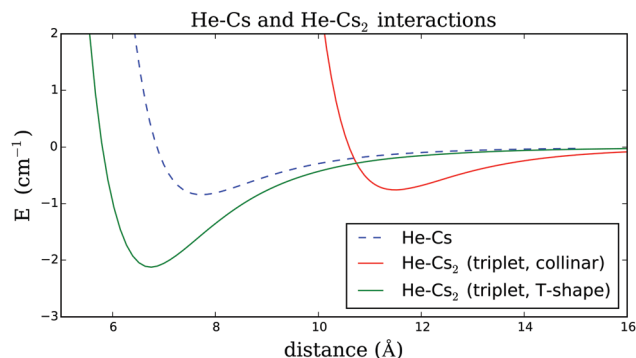
Fig. 5 One-dimensional plots of the pair potentials used for the generation of $U_{ext}[\rho]$ for the He-DFT calculations. For the Cs_2–He interaction the two extreme cases of a collinear ($\phi = 0°$) and a T-shaped geometry ($\phi = 90°$) are plotted.

Table 4 Characteristics of the pair potentials used in the He-DFT approach

Interaction	r_{min} (Å)	E (cm^{-1})	Ref.
Cs–He	7.73	−0.84	46
Cs_2–He, collinear	11.52	−0.76	47
Cs_2–He, T-shaped	6.75	−2.13	47
C_{60}–He	6.76	56.66	42 (fit)

ref. 47. The characteristics of all relevant curves are summarized in Table 4.

Following the diatomics-in-molecules (DIM) approach,[48,49] a three-dimensional estimate of the He–Cs_2 pair potential can be obtained from the cuts provided in Fig. 5 *via* an angular-dependent mixing of both curves, either by

$$U(r,\phi) = U_T(r) \cos^2 \phi + \tfrac{1}{2}[U_{coll}(r) + U_T(r)] \sin^2 \phi, \quad (4)$$

in the case of the Cs_2 axis being perpendicular to the C_3 axis of the fullerene, or by

$$U(r,\phi) = U_T(r) \sin^2 \phi + U_{coll}(r) \cos^2 \phi \quad (5)$$

if the Cs_2 axis is parallel to the C_3 axis of the fullerene, with $U_T(r)$ as the curve corresponding to the T-shaped structure, $U_{coll}(r)$ as the curve corresponding to the collinear structure, and the angle ϕ as defined above. This linear combination of both contributions in the first case reflects a flat positioning of the Cs_2 molecule on the surface of the droplet. A similar approach has been performed in the past *e.g.* for the explanation of spectra caused by electronic p-type excitations of heliophobic atoms residing on the droplet surface,[50] and it is a well-established method in the He-droplet community.[51–56] The average of both potentials in eqn (4) occurs due to the breaking of the cylindrical symmetry in the diatomic picture.

3.6 He droplet simulations

The aim of this section is the evaluation of a reaction pathway for the interaction of Cs or Cs_2 with C_{60} in the environment of

superfluid helium at a temperature of 0.38 K. We simulate a situation which has been realized recently in He droplet experiments of Renzler *et al.*,[7] in which a sequential pickup of C_{60} fullerenes and Cs atoms was studied by electron ionization mass spectrometry. While heliophilic fullerenes immerse into the droplet completely, the heliophobic alkali metal atoms are known to reside on the droplet surface due to their diffuse valence electron density. This spatial separation, which occurs in cases where C_{60} pickup takes place before Cs pickup, together with the hindered mobility of the dopants on and in the droplet,[57] gives rise to the question whether a reaction between the fullerene and the alkali metal atom can take place or not. An interesting observation of this recent experiment is that Cs_2 seems to react with the fullerene, while a single Cs atom does not.

From the potential curves shown in Fig. 1 and 2 it can be seen that the interaction of a single Cs atom with C_{60} is much weaker than the interaction of Cs_2 with C_{60}. Assuming a full quenching of charge transfer due to the helium environment we obtained the curves shown in Fig. 3, in which the spin-parallel configuration of Cs_2, which is expected to be the dominating spin state on He droplets,[58,59] still shows a bound state, while the atomic curve does not. However, this picture is yet incomplete as we have not taken the direct impact of sterical hindrance into consideration, an effect which occurs due to embedding in superfluid helium. The aim of this last computational study is to evaluate this reaction barrier by calculating and comparing the total energies of the systems He_N–Cs–C_{60} and He_N–Cs_2–C_{60} as a function of the distance between the two dopants. In order to do that we proceed as follows:

First, we create three-dimensional interaction potentials for all dopants from the potential curves given in Fig. 4 and 5. In the case of the 'spherical' particles (Cs and C_{60}) the potentials can be generated *via* a simple pair summation over the corresponding potential curves for the interaction with a single He atom. In the case of Cs_2, we use the analytical potential $U(r,\phi)$ introduced above. In a second step, we evaluate the total energy of a multiply-doped He droplet consisting of $N = 2000$ He atoms *via* He-DFT as a function of the distance between the heliophilic and the heliophobic dopant. Three example density distributions for a distance of 20 Å are shown in Fig. 6 as contour plots of planar cuts through the system. Note the helium shell of exceptionally high density which surrounds the fullerene. By repeating the He-DFT energy evaluations for intermolecular distances from 5 to 35 Å we obtain the barriers plotted in Fig. 7. We find a barrier of approximately 400 cm^{-1} for a single atom, while the barriers for the Cs_2 dimer are about three times higher due to the larger perturbation. The maximum of the barrier for the T-shaped configuration is not fully captured by the given scanning range but irrelevant since the Cs_2–C_{60} interaction potential itself is already fully repulsive at a short distance of 5 Å. After setting these energies to zero at the asymptote of infinite distance between Cs_x and the fullerene inside the He-droplet, this energy correction is added to the interaction energies between the two dopants evaluated in the previous sections.
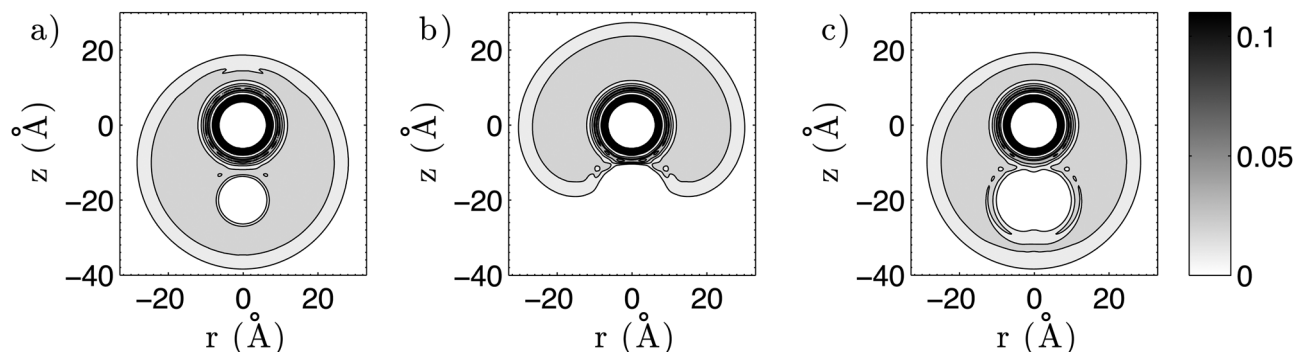
Fig. 6 Contour plots of the helium density for a distance of 20 Å between the fullerene and (a) a single Cs atom, (b) the triplet Cs_2 dimer in a collinear configuration, (c) the triplet Cs_2 dimer in a T-shaped configuration. The density is plotted in units of $Å^{-3}$. Note that the bulk value for the density of liquid helium is 0.02185 atoms per $Å^3$.

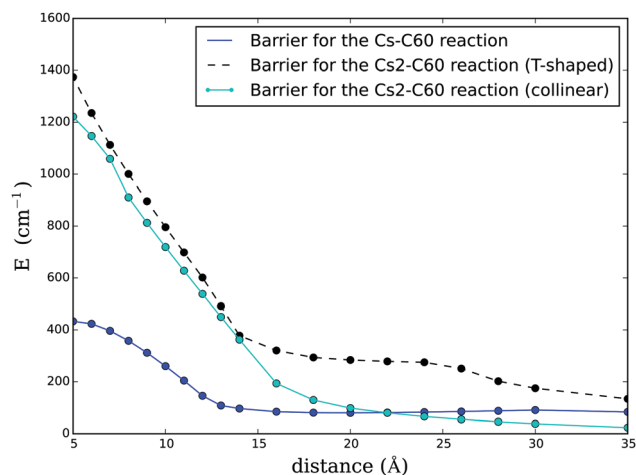**Fig. 7** Estimations of the energy barriers which occur due to sterical hindrance during the reaction of Cs or Cs_2 with C_{60} inside a helium droplet formed by 2000 He atoms, evaluated using orbital-free helium density functional theory.

If we naively assume that the interaction between the fullerene and Cs_x is not quenched at all by the surrounding helium, we can perform this correction by a simple pointwise summation of the He-DFT results and the free-gas curves of Fig. 1 and 2. The results of this first assumption are already plotted in the same figures as dashed lines. As can be seen, the corrections are marginal compared to binding energies in the range of thousands of wavenumbers and cannot explain any preference for the Cs_2–C_{60} reaction over the Cs–C_{60} reaction. On the other hand, if we make the assumption of a fully quenched charge transfer, we have to apply our pointwise correction to the potential curves plotted in Fig. 3. Here, the situation is completely different due to the similar magnitude of the remaining weak attractive interaction between triplet Cs_2 and the barrier due to the sterical hindrance: the helium environment has a huge impact on the reaction. After this final correction, the weakly bound state disappears even for triplet Cs_2. Note that this outcome is sensitive to the actual depth of the charge-constrained potential curve, which might still deviate from the exact curve by a few hundred wavenumbers due to lack of correlation. Indeed,

preliminary calculations of the Cs_2/C_{60} dispersion interaction at the DFT-SAPT level indicate that the well-depth could be underestimated by up to 200 cm^{-1}. However, since the helium-induced correction caused by sterical hindrance lies in the range of about 1200 cm^{-1}, it is unlikely that an improved, more accurate description of the charge-constrained state will alter this result. From this, and the experimentally proven fact that the Cs_2–C_{60} reaction takes place, it can be concluded that an electron transfer process must be involved in the overall reaction, despite the dense helium environment. Although our studies do not include any direct description of how or to which extend this transfer is affected by the helium environment, the two extremes described above can be interpreted as boundaries for the actual process. In the light of these two extremes, and given the recent findings of our experimental colleagues, reality seems to be closer to the second case, where charge transfer is significantly quenched but still determines whether the reaction takes place or not. This links our current efforts to much earlier studies on the concept of a 'harpoon mechanism', where long-range electron transfer is postulated near crossing points of neutral van der Waals and ionic potential energy curves.[60] It remains an open question if this transfer of charge needs to be described *via* exciplex formation involving He atoms, similar to electron hopping processes between dopants in a rare gas matrix, for example induced by cooperative photoadsorption,[61,62] or if a vibrational coupling of the neutral and the ionic states of Cs_x–C_{60} through the helium environment is sufficient. In any case, future studies on this subject are needed which also capture the dynamics of this fascinating phenomenon.

4 Conclusions

The interaction of a single Cs atom or a Cs_2 dimer with a C_{60} fullerene has been studied in gas phase as well as by embedding in superfluid helium *via* a combination of quantum chemistry methods (DFT and MCSCF) and orbital-free bosonic helium density functional theory. This study was triggered by the recent experimental finding that a single Cs atom, which is heliophobic, does not seem to react with a heliophilic fullerene

1348 | *Phys. Chem. Chem. Phys.*, 2017, **19**, 1342–1351

This journal is © the Owner Societies 2017

embedded in helium nanodroplets, while a Cs_2 dimer, on the other hand, seems to be able to reach the fullerene inside the droplet. We found that the $a^3\Sigma_u^+$ state of Cs_2 is bound to a fullerene with a dissociation energy of more than 17 300 cm^{-1}, which is about 4600 cm^{-1} higher than the dissociation energy of the $X^1\Sigma_g^+$ ground state, while a single Cs atom, on the other hand, is only bound by about 11 100 cm^{-1}. In order to estimate the effect of helium embedding on the reaction pathways, which we approximated by a linear approximation along the C_3 axis of the fullerene, we corrected the obtained curves in two ways.

The first correction accounted for a quenching of charge transfer. Since we do not know the impact of helium embedding on the mobility of electrons we made the two extreme assumptions of an unquenched and a fully quenched electron transfer. The first scenario is realized by simple gas-phase computations, while the second is computed *via* charge-constrained DFT calculations, which enforced the charge neutrality of both fragments at all times, or *via* two-state MCSCF calculations including long-range dispersion corrections. In the latter case, we obtained a weakly bound state (160 cm^{-1}) of triplet multiplicity for C_{60}–Cs_2 in a T-shaped arrangement, while a single Cs atom shows a fully repulsive interaction.

The second correction accounted for the spatial hindrance due to the extrusion of helium upon approach of the two reactants. Based on careful fits of *ab initio* data for the interactions of helium with both dopants we modeled external potentials for the helium-DFT calculation of total energies for the systems He$_{2000}$–C_{60}–Cs and He$_{2000}$–C_{60}–Cs_2, and used them for energy corrections of the free-gas and charge-transfer-quenched curves. These corrections are of the order of a few hundred wavenumbers, which turned out to be fully negligible in the case of the free-gas curves, but crucial for the constrained curves: after inclusion the charge-neutral C_{60}–Cs_2 state also becomes fully repulsive. From this finding and the experimental fact that the C_{60}–Cs_2 reaction takes place we conclude that a minimal charge transfer must occur despite embedding in superfluid helium. We further assume that such an electron transfer process is considerably quenched, but it tips the scale regarding the overall reactivity: it lets the dimer react but prevents the atom from approaching the fullerene.

Appendix

A pairwise potential model for the He/C_{60} interaction

An additive pairwise potential model has been designed to fit the dispersionless and dispersion contributions to the accurate DFT-SAPT He–C_{60} interaction energies calculated by Hesselmann and Korona.[42] Our potential model can be viewed as an extended version of that previously developed to account for anti-corrugation effects in the interaction of He atoms with metallic surfaces.[63] It also extends the Lennard-Jones functional developed by Carlos and Cole,[64,65] to account for corrugation effects in the adsorption of noble-gases onto the graphite surface.

Our pairwise potential model exploits the fact that DFT-SAPT interaction energies can be decomposed in dispersionless

($E_{int}^{disp\text{-}less}$) and dispersion contributions (E_{int}^{disp}). The dispersion energies can be very well fitted by means of the D_{as} functional of Szalewicz and collaborators,[66–68] but modulated by a corrugation scaling amplitude:

$$E_{int}^{disp}(\{\mathbf{R}_{HeC}\}) = -\sum_{C}\left[1 + \gamma_A\left(1 - \frac{3}{2}\cos^2\theta_C\right)\right]$$
$$\times \sum_{n=6,8}\frac{\sqrt{C_n^{He}C_n^C}}{R_{HeC}^n}f_n\left(\sqrt{\beta_{He}\beta_C}R_{HeC}\right), \quad (6)$$

where R_{HeC} stands for the distance between the He atom and one fullerene C atom, θ_C is the angle between the vector going from the C_{60} mass center to the He atom and the vector $\mathbf{R}_{HeC}$ from the He atom to the same C atom. The sum in the second term (the D_{as} function) runs over all C atoms of C_{60} and the terms f_n stand for the damping functions of Tang and Toennies.[69] The dimensionless factor γ_A in the first term measures the anti-corrugation strength, when γ_A bears a negative value (-0.5 for the He–C_{60} interaction). This means that dispersion becomes more attractive when the He atom is on top of fullerene C atoms.

When noble-gas atoms are adsorbed onto non-metallic surfaces (see, *e.g.*, ref. 70 and 71), dispersionless energy contributions are repulsive in the short-range and scale exponentially as the distance between the interacting species decrease. They can be fitted to the pairwise additive functional:

$$E_{int}^{disp\text{-}less}(\{\mathbf{R}_{HeC}\}) = \sum_{C}\left[1 + \gamma_R\left(1 - \frac{6}{5}\cos^2\theta_C\right)\right]$$
$$\times Ae^{(-\alpha R_{HeC} - \beta R_{HeC}^2)}, \quad R_{HeC} < R_c$$
$$= 0, \quad\quad\quad\quad R_{HeC} > R_c \quad (7)$$

where R_c is the cut-off distance. The dimensionless factor γ_R modulates the corrugation amplitude. For anti-corrugated cases, the interaction energy is less repulsive directly above the fullerene C atoms, with $\cos^2\theta_C$ adopting a value close to unity. This is translated in positive γ_R values. The opposite holds when the interaction energy becomes less repulsive for the noble-gas atoms adsorbed on "hollow" sites (*e.g.*, the centers of the pentagons and hexagons in C_{60}). This is the case for the He–C_{60} interaction ($\gamma_R = -0.8$).

Dispersion-corrected MCSCF calculations of neutral states

Using the Molpro package,[22] we have performed additional Hartree–Fock and two-state multi-configurational self-consistent-field (MCSCF)[18,19] calculations to characterize the interaction potential between Cs and $Cs_2(^a\Sigma_u^+)$ and C_{60} neutral fragments, with the Cs–Cs axis oriented perpendicular to the C_3 axis. For cesium atoms we used the same basis set as in the B97M-V calculations (*vide supra*). The polarized correlation-consistent double-ζ basis of Woon and Dunning, Jr[72] (cc-pVDZ) was adopted for fullerene carbon atoms instead. Test calculations in computing the Cs_2/benzene interaction potential showed that the enlargement of the carbon basis set from cc-pVDZ to the polarized correlation-consistent triple-ζ basis increases the

This journal is © the Owner Societies 2017

Phys. Chem. Chem. Phys., 2017, **19**, 1342–1351 | **1349**

well-depth by *ca.* 10%. A minimal active space was used in the two-state-MCSCF calculations to account for the main non-dynamical correlation effects, consisting of the 5s orbitals from the Cs and Cs_2 species along with frontier π-type molecular orbitals of the C_{60} system.

To estimate the dynamical correlation contribution to the interaction, identified as dispersion, we adopted the following strategy: first, coupled-cluster singles, doubles and non-iterative triples [CCSD(T)] calculations[20] were performed to calculate the Cs/benzene and $Cs_2(^a\Sigma_u^+)$/benzene interactions. In the relevant potential region, it was checked *via* a Mulliken population analysis that, for a perpendicular orientation of the Cs–Cs internuclear distance to the C_6 axis, the $Cs_2(^a\Sigma_u^+)$ and Cs fragments are kept neutral (see the ESI† for details). Next, following a similar strategy as was presented in previous studies (see ref. 73–75), correlation energy contributions in the long-range potential region were fitted to the effective interatomic function D_{as} (the same as in eqn (6), but excluding the corrugation factor). Finally, the dispersion parameters extracted from the benzene model system were used to calculate the dispersion contributions to the Cs/C_{60} and $Cs_2(^a\Sigma_u^+)/C_{60}$ interactions. These contributions were added to the MCSCF interaction energies.

Acknowledgements

References

1 J. P. Toennies and A. F. Vilesov, *Angew. Chem., Int. Ed.*, 2004, **43**, 2622–2648.

2 J. Tiggesbäumker and F. Stienkemeier, *Phys. Chem. Chem. Phys.*, 2007, **9**, 4748–4770.

3 C. Callegari and W. E. Ernst, in *Handbook of High Resolution Spectroscopy*, ed. F. Merkt and M. Quack, John Wiley & Sons, Chichester, 2011.

4 M. Mudrich and F. Stienkemeier, *Int. Rev. Phys. Chem.*, 2014, **33**, 301–339.

5 J. Nagl, G. Auböck, A. W. Hauser, O. Allard, C. Callegari and W. E. Ernst, *Phys. Rev. Lett.*, 2008, **100**, 063001.

6 J. Nagl, G. Auböck, A. W. Hauser, O. Allard, C. Callegari and W. E. Ernst, *J. Chem. Phys.*, 2008, **128**, 154320.

7 M. Renzler, M. Daxner, L. Kranabetter, A. Kaiser, A. W. Hauser, W. E. Ernst, A. Lindinger, R. Zillich, P. Scheier and A. M. Ellis, *J. Chem. Phys.*, 2016, **145**, 181101.

8 J. Poms, A. W. Hauser and W. E. Ernst, *Phys. Chem. Chem. Phys.*, 2012, **14**, 15158–15165.

9 F. Weigend and R. Ahlrichs, *Phys. Chem. Chem. Phys.*, 2005, **7**, 3297–3305.

10 D. Rappoport and F. Furche, *J. Chem. Phys.*, 2010, **133**, 134105.

11 T. Leininger, A. Nicklass, W. Küchle, H. Stoll, M. Dolg and A. Bergner, *Chem. Phys. Lett.*, 1996, **255**, 274–280.

12 N. Mardirossian and M. Head-Gordon, *J. Chem. Phys.*, 2014, **140**, 18A527.

13 A. D. Becke, *J. Chem. Phys.*, 1997, **107**, 8554.

14 O. A. Vydrov and T. Van Voorhis, *J. Chem. Phys.*, 2010, **133**, 244103.

15 S. F. Boys and F. Bernardi, *Mol. Phys.*, 1970, **19**, 553–566.

16 A. D. Rabuck and G. E. Scuseria, *J. Chem. Phys.*, 1999, **110**, 695.

17 Q. Wu and T. Van Voorhis, *Direct Calculation of Electron Transfer Parameters through Constrained Density Functional Theory*, American Chemical Society, 2006, vol. 110.

18 H.-J. Werner and W. Meyer, *J. Chem. Phys.*, 1980, **73**, 2342.

19 P. J. Knowles and H.-J. Werner, *Chem. Phys. Lett.*, 1985, **115**, 219.

20 J. D. Watts, J. Gauss and R. J. Bartlett, *J. Chem. Phys.*, 1993, **98**, 8718–8733.

21 Y. Shao, Z. Gan, E. Epifanovsky, A. T. Gilbert, M. Wormit, J. Kussmann, A. W. Lange, A. Behn, J. Deng, X. Feng, D. Ghosh, M. Goldey, P. R. Horn, L. D. Jacobson, I. Kaliman, R. Z. Khaliullin, T. Kuś, A. Landau, J. Liu, E. I. Proynov, Y. M. Rhee, R. M. Richard, M. a. Rohrdanz, R. P. Steele, E. J. Sundstrom, H. L. Woodcock, P. M. Zimmerman, D. Zuev, B. Albrecht, E. Alguire, B. Austin, G. J. O. Beran, Y. a. Bernard, E. Berquist, K. Brandhorst, K. B. Bravaya, S. T. Brown, D. Casanova, C.-M. Chang, Y. Chen, S. H. Chien, K. D. Closser, D. L. Crittenden, M. Diedenhofen, R. a. DiStasio, H. Do, A. D. Dutoi, R. G. Edgar, S. Fatehi, L. Fusti-Molnar, A. Ghysels, A. Golubeva-Zadorozhnaya, J. Gomes, M. W. Hanson-Heine, P. H. Harbach, A. W. Hauser, E. G. Hohenstein, Z. C. Holden, T.-C. Jagau, H. Ji, B. Kaduk, K. Khistyaev, J. Kim, J. Kim, R. a. King, P. Klunzinger, D. Kosenkov, T. Kowalczyk, C. M. Krauter, K. U. Lao, A. Laurent, K. V. Lawler, S. V. Levchenko, C. Y. Lin, F. Liu, E. Livshits, R. C. Lochan, A. Luenser, P. Manohar, S. F. Manzer, S.-P. Mao, N. Mardirossian, A. V. Marenich, S. a. Maurer, N. J. Mayhall, E. Neuscamman, C. M. Oana, R. Olivares-Amaya, D. P. O'Neill, J. a. Parkhill, T. M. Perrine, R. Peverati, A. Prociuk, D. R. Rehn, E. i. Rosta, N. J. Russ, S. M. Sharada, S. Sharma, D. W. Small, A. Sodt, T. Stein, D. Stück, Y.-C. Su, A. J. Thom, T. Tsuchimochi, V. Vanovschi, L. Vogt, O. Vydrov, T. Wang, M. a. Watson, J. Wenzel, A. White, C. F. Williams, J. Yang, S. Yeganeh, S. R. Yost, Z.-Q. You, I. Y. Zhang, X. Zhang, Y. Zhao, B. R. Brooks, G. K. Chan, D. M. Chipman, C. J. Cramer, W. a. Goddard, M. S. Gordon, W. J. Hehre, A. Klamt, H. F. Schaefer, M. W. Schmidt, C. D. Sherrill, D. G. Truhlar, A. Warshel, X. Xu, A. Aspuru-Guzik, R. Baer, A. T. Bell, N. a. Besley, J.-D. Chai, A. Dreuw, B. D. Dunietz, T. R. Furlani, S. R. Gwaltney, C.-P. Hsu, Y. Jung, J. Kong, D. S. Lambrecht, W. Liang, C. Ochsenfeld, V. a. Rassolov, L. V. Slipchenko, J. E. Subotnik, T. Van Voorhis, J. M. Herbert, A. I. Krylov, P. M. Gill and M. Head-Gordon, *Mol. Phys.*, 2015, **113**, 184–215.

1350 | *Phys. Chem. Chem. Phys.*, 2017, **19**, 1342–1351

This journal is © the Owner Societies 2017

22 H. J. Werner, P. J. Knowles, G. Knizia, F. R. Manby, M. Schütz, P. Celani, T. Korona, R. Lindh, A. O. Mitrushchenkov, G. Rauhut, et al., MOLPRO, version 2012.1, a package of ab initio programs, see http://www.molpro.net.

23 G. Höning, M. Czajkowski, M. Stock and W. Demtröder, J. Chem. Phys., 1979, 71, 2138–2149.

24 M. Raab, H. Weickenmeier and W. Demtröder, Chem. Phys. Lett., 1982, 88, 377–383.

25 B. Assadollahzadeh, C. Thierfelder and P. Schwerdtfeger, Phys. Rev. B: Condens. Matter Mater. Phys., 2008, 78, 245423.

26 I. Moullet, W. Andreoni and P. Giannozzi, J. Chem. Phys., 1989, 90, 7306–7312.

27 D. Li, F. Xie, L. Li, S. Magnier, V. Sovkov and V. Ivanov, Chem. Phys. Lett., 2007, 441, 39–42.

28 A. W. Hauser, G. Auböck and W. E. Ernst, Vibronic Interactions and the Jahn–Teller Effect, Springer Netherlands, Dordrecht, 2012, pp. 301–316.

29 F. Dalfovo, A. Lastri, L. Pricaupenko, S. Stringari and J. Treiner, Phys. Rev. B: Condens. Matter Mater. Phys., 1995, 52, 1193.

30 F. Ancilotto, M. Barranco, F. Caupin, R. Mayol and M. Pi, Phys. Rev. B: Condens. Matter Mater. Phys., 2005, 72, 214522.

31 F. Caupin, F. Ancilotto, M. Barranco, R. Mayol and M. Pi, J. Low Temp. Phys., 2007, 148, 731–736.

32 The geometry of the C_{60} molecule was optimized at the same level of theory.

33 G. Auböck, J. Nagl, C. Callegari and W. E. Ernst, J. Phys. Chem. A, 2007, 111, 7404–7410.

34 R. Pérez de Tudela, D. López-Durán, T. González-Lezana, G. Delgado-Barrio, P. Villarreal, F. A. Gianturco and E. Yurtsever, J. Phys. Chem. A, 2011, 115, 6892–6902.

35 A. S. Hira and A. K. Ray, Phys. Rev. A: At., Mol., Opt. Phys., 1996, 54, 2205–2215.

36 J. Deigmayr, M. Aymar, R. Wster, M. Weidemüller and O. Dulieu, J. Chem. Phys., 2008, 129, 064309.

37 M. D. Gregorie, I. Hromada, W. F. Holmgren, R. Trubko and A. D. Cronin, Phys. Rev. A: At., Mol., Opt. Phys., 2008, 92, 052513.

38 R. Antoine, D. Rayane, E. Benichou, P. Dugourd and M. Broyer, Eur. Phys. J. D, 2000, 12, 147–151.

39 S. Grimme, J. Comput. Chem., 2006, 27, 1787–1799.

40 N. Mardirossian and M. Head-Gordon, Phys. Chem. Chem. Phys., 2014, 16, 9904–9924.

41 J. D. Watts, J. Gauss and R. J. Bartlett, J. Chem. Phys., 1993, 98, 8718–8733.

42 A. Hesselmann and T. Korona, Phys. Chem. Chem. Phys., 2010, 13, 732–743.

43 A. J. Misquitta, B. Jeziorski and K. Szalewicz, Phys. Rev. Lett., 2003, 91, 033201.

44 A. Hesselmann and G. Jansen, Chem. Phys. Lett., 2003, 367, 778.

45 A. W. Hauser and M. P. de Lara-Castells, J. Phys. Chem. Lett., 2016, 7, 4929–4935.

46 S. H. Patil, J. Chem. Phys., 1991, 94, 8089–8095.

47 R. Prosmiti, G. Delgado-Barrio, P. Villarreal, E. Yurtsever, E. Coccia and F. A. Gianturco, J. Phys. Chem. A, 2009, 113, 14718–14729.

48 F. O. Ellison, J. Chem. Phys., 1983, 78, 5024–5030.

49 F. O. Ellison, J. Am. Chem. Soc., 1963, 85, 3540–3544.

50 M. Ratschek, J. V. Pototschnig, A. W. Hauser and W. E. Ernst, J. Phys. Chem. A, 2014, 118, 6622–6631.

51 D. Mateo, A. Hernando, M. Barranco, E. Loginov, M. Drabbels and M. Pi, Phys. Chem. Chem. Phys., 2013, 15, 18388–18400.

52 M. Leino, A. Viel and R. E. Zillich, J. Chem. Phys., 2011, 134, 024316.

53 A. Hernando, M. Barranco, R. Mayol, M. Pi and M. Krosnicki, Phys. Rev. B: Condens. Matter Mater. Phys., 2008, 77, 024513.

54 A. Hernando, M. Barranco, R. Mayol, M. Pi and F. Ancilotto, Phys. Rev. B: Condens. Matter Mater. Phys., 2008, 78, 184515.

55 O. Bunermann, G. Droppelmann, A. Hernando, R. Mayol and F. Stienkemeier, J. Phys. Chem. A, 2007, 111, 12684–12694.

56 M. Mella, M. C. Colombo and G. Morosi, J. Chem. Phys., 2002, 117, 9695–9702.

57 A. W. Hauser, A. Volk, P. Thaler and W. E. Ernst, Phys. Chem. Chem. Phys., 2015, 17, 10805–10812.

58 F. Stienkemeier, W. E. Ernst, J. Higgins and G. Scoles, J. Chem. Phys., 1995, 102, 615–617.

59 W. E. Ernst, R. Huber, S. Jiang, R. Beuc, M. Movre and G. Pichler, J. Chem. Phys., 2006, 124, 024313.

60 J. L. Magee, J. Chem. Phys., 1940, 8, 687–698.

61 M. E. Fajardo and V. A. Apkarian, J. Chem. Phys., 1986, 85, 5660–5681.

62 M. E. Fajardo and V. A. Apkarian, J. Chem. Phys., 1988, 89, 4102–4123.

63 M. P. de Lara-Castells, R. Fernández-Perea, F. Madzharova and E. Voloshina, J. Chem. Phys., 2016, 144, 244707.

64 L. W. Brunch, M. C. Cole and E. Zaremba, Physical Adsorption: Forces and Phenomena, Clarendon Press, Oxford, 1997.

65 W. E. Carlos and M. W. Cole, Surf. Sci., 1980, 91, 339–357.

66 K. Pernal, R. Podeszwa, K. Patkowski and K. Szalewicz, Phys. Rev. Lett., 2009, 103, 263201.

67 R. Podeszwa and K. Szalewicz, J. Chem. Phys., 2012, 136, 161102.

68 R. Podeszwa, K. Pernal, K. Patkowski and K. Szalewicz, J. Phys. Chem. Lett., 2010, 1, 550–555.

69 K. T. Tang and J. P. Toennies, J. Chem. Phys., 1984, 80, 3726–3741.

70 M. P. de Lara-Castells, M. Bartolomei, A. O. Mitrushchenkov and H. Stoll, J. Chem. Phys., 2015, 143, 194701.

71 M. P. de Lara-Castells, H. Stoll and A. O. Mitrushchenkov, J. Phys. Chem. A, 2014, 118, 6367–6384.

72 D. E. Woon and T. H. Dunning, J. Chem. Phys., 1994, 100, 2975–2988.

73 M. P. de Lara-Castells, H. Stoll, B. Civalleri, M. Causà, E. Voloshina, A. O. Mitrushchenkov and M. Pi, J. Chem. Phys., 2014, 141, 151102.

74 M. P. de Lara-Castells, N. F. Aguirre, H. Stoll, A. O. Mitrushchenkov, D. Mateo and M. Pi, J. Chem. Phys., 2015, 142, 131101.

75 M. P. de Lara-Castells, A. O. Mitrushchenkov and H. Stoll, J. Chem. Phys., 2015, 143, 102804.

This journal is © the Owner Societies 2017

Phys. Chem. Chem. Phys., 2017, 19, 1342–1351 | 1351